J Mater Sci (2009) 44:6182–6186
DOI 10.1007/s10853-009-3857-1

Plastic anisotropy and strain-hardening behavior of Mg–6%Li–1%Zn alloy thin sheet at elevated temperatures

Horng-Yu Wu · Geng-Zhong Zhou

Received: 1 May 2009 / Accepted: 27 August 2009 / Published online: 4 September 2009

Abstract An Mg–Li–Zn (designated as LAZ61) alloy containing about 6 wt% of Li has been prepared by melting and solidification in a carbon steel crucible, and extruded at a billet preheating temperature of 200 °C. The extruded plate was then cold-rolled to a final thickness of 0.6 mm with a total reduction of approximately 82%. Tensile tests were carried out in the rolling and transverse directions and at various temperatures to explore the effects of anisotropy and temperature on mechanical properties and strain-hardening behavior. Kocks–Mecking type plots were used to illustrate different stages of strain hardening. Anisotropic behavior of LZ61 sheet were observed in the mechanical properties at all test temperatures due to the development of texture in α phase during cold-rolling and a low content of BCC β phase. The cold-rolled LZ61 alloy sheet showed stage II and stage III strain-hardening behavior at test temperatures of room temperature and 100 °C. The specimens tested at 200 °C did not show stage II strain hardening. Higher initial strain-hardening rates were observed in the transverse direction as a result of the cold-rolled fibrous structure providing more strong barriers to the dislocation movement.

Introduction

Strain-hardening behavior is one of the important considerations in the evaluation of plastic deformation of materials [1], and strain-hardening exponent is also the most important factor that influences stretchability, when stretching predominates in the forming processes [2–4]. The strain-hardening behavior of cubic metals is fairly well understood and accumulation of a forest of dislocations is the dominant hardening mechanism [5–8]. Hexagonal metals present a more complex case due to their low symmetry, which restricts the number of slip systems [5], and their strong plastic anisotropy. In Mg and its alloys, strain-hardening behavior is observed as in face-centered cubic (FCC) crystals [9–13]. At higher temperatures, a dynamic balance between hardening and softening is observed in ZE41 and QE22 magnesium alloys. Double cross slip of <c + a> dislocations is assumed as the mechanism leading to softening [14]. The analysis of AM60 Mg alloy indicates that hardening involves solid solution hardening and interaction with forest dislocations and non-dislocation obstacles such as second phase particles [15]. The strain-hardening rate of Mg–8%Li alloy is significantly influenced by the deformation temperature [16].

Among Mg alloys, magnesium–lithium (Mg–Li) alloys, as the lightest structural metallic materials, are attractive for a large amount of applications. The Mg–Li phase diagram [17] indicates that when the Li content is between ~5.5 and 11.5 wt%, the BCC structured β phase of the Li solid solution coexists with the HCP α phase of the Mg solid solution. The β single phase structure exists for Li contents higher than 11 wt%. The crystal lattice axes ratio, *c*/*a*, of the HCP α phase with Li addition decreases such that slip between crystal planes become less difficult [18]. The coexistence of the β phase could improve formability of the Mg–Li alloy at room temperature.

The deformation behavior of Mg–Li alloys has long been investigated [19–25]. However, few studies have been carried out to examine the strain-hardening behavior [16, 19], though it is important to develop new Mg–Li alloys

H.-Y. Wu (✉) · G.-Z. Zhou
Department of Mechanical Engineering, Chung-hua University, Hsinchu 30012, Taiwan, ROC
e-mail: ncuwu@chu.edu.tw

with suitable mechanical characteristics. The aim of the present work is to study the influence of temperature and anisotropy on tensile properties of the Mg–6%Li–1%Zn (wt%) alloy thin sheet, to explore the strain-hardening behavior at elevated temperatures.

Materials and experimental procedures

The Mg–Li alloy was melted in a high-vacuum electric induction furnace under an argon atmosphere and then cast into an ingot with a cylindrical shape of 200 mm in diameter and 400 mm in height. The analyzed chemical composition of the cast alloy by use of induction coupled plasma (ICP) and Spark Optical Emission Spectrometry (Spark-OES) apparatuses was (wt%) Mg–5.8Li–0.51Zn (designated as LZ61). The cylindrical ingot was first homogenized at 300 °C for 12 h and then extruded into a plate with a thickness of 3.3 mm at an ingot preheating temperature of 200 °C. The extruded plate was flat-rolled at room temperature to a final thickness of 0.6 mm with a total reduction of approximately 82%; about 5% reduction in thickness for each pass during rolling.

Uniaxial tension tests were carried out in the rolling direction (RD), transverse direction (TD), and an intermediate (45°) on three samples for each test. The gauge length and width of the tensile specimens were 50 and 6 mm, respectively. The specimens were tested at room temperature, 100 and 200 °C at an initial strain rate of 1.67×10^{-3} s^{-1}.

The specimens for microscopic examination were prepared by conventional metallographic techniques. The polished specimens were etched for 1–5 s in the etchant of 5 g picric acid, 10 mL acetic acid, and 95 mL ethyl alcohol. Optical microscope was used to examine the microstructure.

Results and discussion

Microstructure of the LZ61 alloy

The as-cast structure of the LZ61 alloy presents a dual-phase microstructure, as given in Fig. 1. β phase is the Li solid solution of low atomic number while the α phase is the Mg solid solution with a higher atomic number. The volume fraction of each phase analyzed by image analyzer is about 92.9% α and 7.1% β, and it is quite consistent with the value estimated from the phase diagram. Figure 2 reveals that the as-rolled structure exhibits fibrous rolling structure, which is a typical plastically deformed structure. α and β phases are elongated and aligned in the RD caused by heavy rolling.

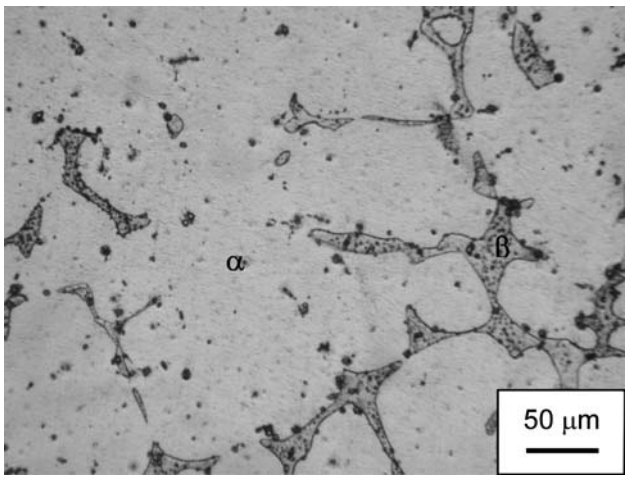

Fig. 1 Optical micrograph of the as-cast microstructure of the LZ61 alloy

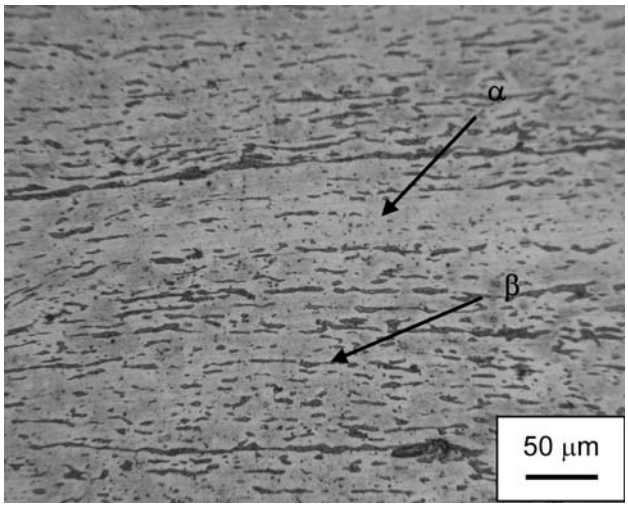

Fig. 2 Optical micrograph of the as-rolled microstructure of the LZ61 alloy

Tensile properties

Figure 3 demonstrates the true stress–strain curves of the LZ61 alloy in RD and TD at various temperatures obtained from the uniaxial tension tests with an initial strain rate of 1.67×10^{-3} s^{-1}. The average values of the strengths and elongation are evaluated as [26]:

$$\text{Average} = \frac{X_{RD} + 2X_{45} + X_{TD}}{4}, \quad (1)$$

where X is the yield stress or the ultimate tensile stress, or the elongation. The average values of the tensile properties tested at various temperatures are listed in Table 1.

Maximum strengthening was observed in the TD at room temperature, as shown in Fig. 3, and elongation in all of the three directions was less than 29%. In comparison

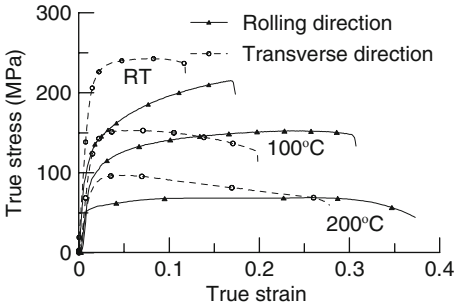

Fig. 3 True stress–strain curves of the LZ61 alloy tested at various temperatures at an initial strain rate of 1.67×10^{-3} s^{-1}

Table 1 Average tensile properties of the LZ61 sheet tested at various temperatures

Property	Room temperature	100 °C	200 °C
Average yield stress (MPa)	146.2	109.1	69.4
Average ultimate tensile stress (MPa)	197.9	131.2	72.1
Average elongation (%)	20.6	34.1	43.9

with the properties at room temperature, the average yield and ultimate strength decrease about 25.4 and 33.7%, respectively, and an increase in average elongation is about 65.5% for testing at a temperature of 100 °C. Significant decreases in strengths were found for testing at a temperature of 200 °C. The average yield and ultimate strength decrease were about 52.5 and 63.6%, respectively, and an increase in average elongation is about 113.1%. The main strengthening effect of Mg–Li alloy is solid solution hardening. The activity of non-basal slip systems and cross-slip of dislocations increases with temperature for Mg–Li alloy; as indicated by Agnew et al. [25]. At higher temperatures, cross-slip becomes a significant recovery process responsible for softening. Therefore, the strengths and the strain-hardening effect decrease and the elongation to failure increases with increasing temperature.

For dual-phase Mg–Li alloys, the quantity of the BCC structured β phase present in the alloy influences the anisotropic behavior. The volume fraction of β phase is approximately 7.1% for LZ61 used in this study. The BCC β phase with a preferred orientation shows anisotropic behavior, but this is less pronounced when compared with a hexagonally close packed α phase with the same degree of texture. This is primarily due to the high degree of symmetry of the cubic β phase, whereas the asymmetry of the hexagonally close packed α phase exacerbates the effects of texture. Therefore, the LZ61 sheet shows noticeable anisotropy of the mechanical behavior due to the development of texture in α phase during cold-rolling and a low content of BCC β phase.

The observed flow stress anisotropy, where TD samples exhibit higher strength than the RD samples at all test temperatures, should be related to the initial rolling texture. Cold-rolled Mg alloy sheets usually have very strong basal texture where the majority of *c*-axes are aligned parallel to the sheet normal direction [25, 27, 28]. As the elongated grains tend to be oriented with their basal planes inclined more toward RD than TD, the Schmid factor $S = \tau/\sigma = \cos\lambda\cos\varphi$ determines how much of the applied normal stress σ will be resolved on the slip system of interest; where λ and φ are the angles between the stress axis and the slip direction and slip plane normal, respectively. Agnew and Duygulu [29] demonstrated that Schmid factor for basal slip of $<a>$ dislocations within the "average" grain in the RD samples is larger than for the TD samples. Thus, the soft basal slip mode can accommodate a more significant fraction of the strain in the RD samples than that of TD and allows easier activation of basal slip by RD tension. The strong basal texture in TD requires activation of non-basal slip, which increases the yield stress [30, 31].

Strain-hardening behavior

A Kocks–Mecking type plot of the strain-hardening behaviors of the specimens tested at various temperatures is illustrated in a plot of strain-hardening rate $\Theta(d\sigma/d\varepsilon)$ versus net flow stress $(\sigma - \sigma_y)$, where σ_y is the (0.2% offset) yield strength, during the plastic deformation at an initial strain rate of 1.67×10^{-3} s^{-1}; as shown in Fig. 4, which is derived from Fig. 3. An initial Θ value that remains at an almost constant strain-hardening rate of approximately 2,300 MPa until the net flow stress reaches nearly 20 MPa was seen in the RD for the specimens tested at room temperature, indicating an initially linear strain hardening of stage II behavior; as illustrated in Fig. 4a. This stage is also observed in polycrystalline FCC metals [5]. Then, Θ decreases with increase in net flow stress exhibiting stage III hardening behavior [5, 32]. A constant Θ value of approximately 5,500 MPa was observed for the samples tested in the TD, and strain hardening of stage III starts at the net flow stress of approximately 9 MPa. Similar results were also observed for the specimens tested at 100 °C; as shown in Fig. 4b. After yielding, the specimens show a high initial and almost constant strain-hardening rate, corresponding to stage II linear hardening, followed by stage III hardening of linearly decreasing hardening rate. However, the specimens tested at 200 °C in all directions do not exhibit any stage II linear hardening behavior, and their stage III with a decreasing Θ occurs immediately after yielding, as shown in Fig. 4c.

The cold-rolled fibrous structure of the LZ61 sheet might have more noticeable impact to the much higher initial strain-hardening rates in the TD than those in the

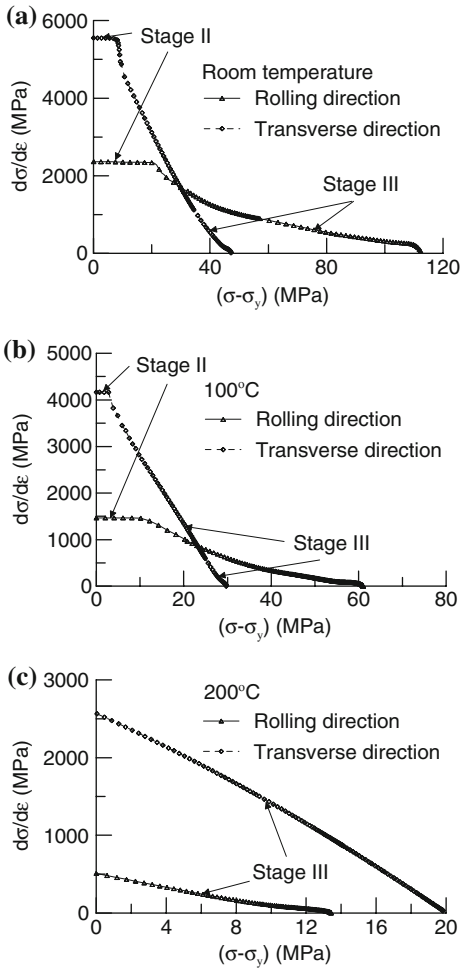

Fig. 4 Strain-hardening rate (Θ) as a function of net flow stress ($\sigma - \sigma_y$) of the LZ61 alloy tested at an initial strain rate of 1.67×10^{-3} s^{-1}. **a** At room temperature, **b** at 100 °C, **c** at 200 °C

other directions. This suggests that much higher activation energy is required for the plastic flow due to very strong barriers to the dislocation movement [32]. As stage II linear hardening is a thermal in nature, the chief mechanism could be related to the evolution of long-range stresses due to dislocation pileups at the grain boundary. Therefore, the elongated grain structure along the RD provides more strong barriers to the dislocation movement in the TD resulting in the higher initial strain-hardening rate in this direction.

The strain-hardening of a material after yielding is related to the dislocation strain field interactions. Thus the Taylor dislocation contribution $\sigma_d = M\eta Gb\rho^{1/2}$ dominates the strain-hardening effect; where ρ is the dislocation density, η a constant, M the Taylor factor, G the shear modulus, and b the Burgers vector. Stress contribution due to dislocation density can be obtained by subtracting the yield stress from the total flow stress and can be written as $\rho^{1/2} \propto \sigma_d = \sigma - \sigma_y$ [13]. Then the applied stress necessary for deformation of the material is proportional to the dislocation density inside the material resulting in a high and nearly constant strain-hardening rate (i.e., stage II linear hardening effect).

The main strengthening effect of LZ61 alloy is solid solution hardening; processes such as cross-slip and climb of dislocations contribute to the softening. The flow stress of the alloy depends on the average dislocation density. The dislocation structure changes during deformation and therefore, the flow stress also changes with strain and temperature. Based on the model proposed by Lukáč and Balík [33], the stress dependence of the strain-hardening rate for polycrystals can be expressed in the following form:

$$\Theta = \frac{A}{\sigma - \sigma_y} + B - C(\sigma - \sigma_y) - D(\sigma - \sigma_y)^3, \quad (2)$$

where the parameter A is connected with the interaction of dislocations with the non-dislocation obstacles; the parameter B relates to the strain-hardening due to the interaction with forest dislocations; the parameter C relates to recovery due to cross slip; the parameter D is connected with the climb of dislocations. The parameter A is expected to increase with increased solute content or the presence of precipitates of second phase particles. The parameter B does not change with temperature, except at higher temperatures, when the activity of non-basal slip increases and it changes the forest dislocation density. Both parameters C and D are related to thermally activated processes and are expected to increase with temperature. At higher temperatures, cross-slip becomes a significant recovery process responsible for softening. The activity of non-basal slip systems and cross-slip of dislocations increases with temperature. This could be the reason for the occurrence of stage III strain-hardening after yielding due to easy cross-slip for LZ61 alloy tested at a temperature of 200 °C.

Conclusions

The effect of plastic anisotropy and temperature on mechanical and strain-hardening behavior of a cold-rolled Mg–Li based alloy sheet with a Li content of approximately 6 wt% was investigated in this study. A dual-phase microstructure including the α matrix plus the distributed β phase was observed in the as-cast LAZ61 alloy. The cold-rolled LZ61 alloy sheet deformed in tensile exhibited noticeable anisotropy of mechanical and strain-hardening behavior. Higher strengthening was observed in the TD at all test temperature. The strengths and the strain-hardening effect decreased and the elongation to failure increased with increasing temperature. Increase in the activity of non-basal slip systems and cross-slip of dislocations with

temperature should be the recovery processes responsible for softening at higher temperatures.

The cold-rolled LZ61 alloy sheet tested at room temperature and 100 °C showed a linear strain-hardening regime over a narrow range of flow stresses in all test directions. A nearly constant strain-hardening rate (i.e., stage II linear hardening effect) appeared after yield. At higher net flow stresses, the strain-hardening rate decreased with the net flow stress and hardening stage III took place. The specimens tested at 200 °C did not exhibit any stage II linear hardening behavior, and their stage III with a decreasing strain-hardening rate occurred immediately after yielding. The activation of non-basal slip and cross-slip should be the reason to suppress the stage II hardening behavior for the specimens tested at 200 °C.

Acknowledgements This work was conducted through grants from National Science Council under the contract No. NSC 97-2221-E-216-010 and Chung-hua University under the contract No. CHU NSC 97-2221-E-216-010.

References

1. Chen XH, Lu L (2007) Scr Mater 57:133
2. Ravi Kumar D, Swaminathan K (1999) Mater Sci Technol 15:1241
3. Mielnik EM (1993) Metalworking science and engineering. McGraw-Hill, Inc, New York
4. Marciniak Z, Kuczynski K, Pokora T (1973) Int J Mech Sci 15:789
5. Kocks UF, Mecking H (2003) Prog Mater Sci 48:171
6. Kuhlmann-Wilsdorf D (2004) Metall Mater Trans A 35:369
7. Kocks UF (1970) Metall Trans 1:1121
8. Mecking H, Kocks UF (1981) Acta Metall 29:1865
9. Lavrentev FF (1980) Mater Sci Eng 46:191
10. Lavrentev FF, Pokhil YA (1975) Mater Sci Eng 18:261
11. Afrin N, Chen DL, Cao X, Jahazi M (2007) Scr Mater 57:1004
12. Cáceres CH, Blake AH (2007) Mater Sci Eng A 462:193
13. del Valle JA, Carreno F, Ruano OA (2006) Acta Mater 54:4247
14. Lukác P, Trojanová Z (2007) Mater Sci Eng A 462:23
15. Máthis K, Trojanová Z, Lukác P, Cáceres CH, Lendvai J (2004) J Alloys Compd 378:176
16. Trojanová Z, Lukác P (2005) J Mater Process Technol 162–163:416
17. Nayeb-Hashemi AA, Clark JB, Pelton AD (1984) Bull Alloy Phase Diagr 5:365
18. Herbstein FH, Averbach BL (1956) Acta Metall 4:407
19. Trojanová Z, Drozd Z, Lukáč P, Chmelík F (2005) Mater Sci Eng A 410–411:148
20. Agnew SR, Horton JA, Yoo MH (2002) Metall Mater Trans A 33:851
21. Takuda H, Matsusaka H, Kikuchi S, Kubota K (2002) J Mater Sci 37:51. doi:10.1023/A:1013133521947
22. Takuda H, Enami T, Kubota K, Hatta N (1999) Mater Sci Eng A 271:251
23. Drozd Z, Trojanová Z, Kúdela S (2004) J Alloys Comp 378:192
24. Kamado S, Kojima Y (1998) Metall Sci Technol 16:45
25. Agnew SR, Yoo MH, Tomé N (2001) Acta Mater 49:4277
26. Narayanasamy R, Sathiya Narayanan C (2005) Mater Sci Eng A 399:292
27. Yukutake E, Kaneko J, Sugamata M (2003) Mater Trans 44:452
28. Styczynski A, Hartig C, Bohlen J, Letzig D (2004) Scr Mater 50:943
29. Agnew SR, Duygulu Ö (2005) Int J Plast 21:1161
30. Koike J, Ohyama R (2005) Acta Mater 53:1963
31. Lou XY, Li M, Boger RK, Agnew SR, Wagoner RH (2007) Int J Plast 23:44
32. Luo J, Mei Z, Tian W, Wang Z (2006) Mater Sci Eng A 441:282
33. Lukáč P, Balík J (1994) Key Eng Mater 97–98:307